Marine Geology 290 (2011) 17–28

Contents lists available at SciVerse ScienceDirect

Marine Geology

journal homepage: www.elsevier.com/locate/margeo

Coastal boulders as evidence for high-energy waves on the Iranian coast of Makran

Majid Shah-hosseini [a,*], Christophe Morhange [a], Abdolmajid Naderi Beni [b], Nick Marriner [a], Hamid Lahijani [b], Mohammadali Hamzeh [b], François Sabatier [a]

[a] Aix-Marseille Univ, CEREGE, UMR 6635 – CNRS, CEREGE, UMR 6635 – IRD, CEREGE, UMR 161 – Collège de France, CEREGE, 13545 Aix en Provence cedex 4, France
[b] Iranian National Institute for Oceanography (INIO), 9 Etemadzadeh St., west Fatemi Av., Tehran, Iran

ARTICLE INFO

Article history:
Received 28 March 2011
Received in revised form 11 October 2011
Accepted 23 October 2011
Available online 29 October 2011

Communicated by J.T. Wells

Keywords:
Iran
Makran
coast
Gulf of Oman
boulder
tsunami
storm
inundation
hazard

ABSTRACT

Coastal boulder deposits attesting to large waves are found along the rocky coast of Makran (Iran) from Chabahar to Lipar. Boulders are either scattered on the rocky coastal platform or accumulated in imbricated clusters. The boulders are mostly rectangular and composed of biogenic calcarenite deriving from the present coastal platform. Significant morphological features observed on the boulders include supratidal karstic pools, sharp broken edges and fractures. Some boulders contain boreholes and shells of marine bivalves, suggesting detachment and transportation from the subtidal zone. The dimensions, elevation and distance from the coastline of 58 representative boulders are documented to estimate their volume, weight and inland displacement. The boulders, weighing up to 18 t, are found up to 6 m above present mean sea level and up to 40 m from the present shoreline. We applied hydrological models to estimate and compare the wave height and inundation distance required to transport the boulders inland. Our results demonstrate that no known or probable storm event on the Makran coast is capable of detaching and transporting the boulders. In contrast, tsunami wave height of 4 m is enough to detach all the boulders from the rocky coast and transport them inland. We conclude that a tsunamigenic origin for boulder deposits is most plausible. Our results imply that the western part of the Makran coast has archived evidence of paleotsunami events, probably generated by large earthquakes at the Makran subduction zone.

1. Introduction

With the expansion of human settlements and infrastructure in coastal areas, hazard assessments and mitigation are critical for developing countries. The 2004 Indian Ocean tsunami, which claimed more than 225,000 lives, demonstrates that the risks posed by tsunamis had been considerably underestimated (Geist et al., 2006). The event sharply focused attention on tsunami hazard assessment, particularly in the Indian Ocean (e.g. Okal and Synolakis, 2008).

The coast of Makran, in the northwestern Indian Ocean, lies in a tectonically active zone and is therefore exposed to coastal hazards. In the absence of reliable instrumental measurements and historical records, geological and geomorphological investigations are essential to evaluate the magnitude and frequency of catastrophic events in the Makran coastal area. The region has been the subject of few published paleotsunami studies. Donato et al. (2008, 2009) have investigated shell layers in Sur lagoon (coast of Oman) and attributed them to the Makran tsunami of 1945. Numerical models have also been developed to assess the tsunami risk of the Makran and adjacent coastlines (Mokhtari, 2005; Heidarzadeh et al., 2008, 2009; Okal and Synolakis, 2008; Jaiswal et al., 2009). Furthermore, the impact of the tropical cyclone Gonu (which happened in June 2007) on coastal areas has been investigated in Iran (Golshani and Taebi, 2008; Dibajnia et al., 2010) and Oman (Fritz et al., 2010). Recently, fieldwork undertaken during the international workshop on assessment and awareness of Makran tsunami hazards (2010), has helped us to improve our knowledge of coastal hazards in Iran. The fieldwork included geological and geomorphological investigations in addition to eyewitness accounts from local inhabitants.

One of the major geomorphological effects of large waves on rocky coasts is the detachment and landward transportation of mega-clasts (Nott, 1997; Mastronuzzi and Sansò, 2000, 2004; Noormets et al., 2002, 2004; Scheffers, 2002; Scheffers and Kelletat, 2003; Morton et al., 2006; Goto et al., 2007; Mastronuzzi et al., 2007; Imamura et al., 2008). Boulder morphometric characteristics such as size, shape, density and displaced distance are investigated in order to evaluate the hydrodynamics of transporting waves (e.g. Nott, 1997, 2003; Noormets et al., 2004). Displaced boulders have been used as indicators of coastal flooding events in different parts of the world, including Indonesia (Paris et al., 2010), the Mediterranean (Mastronuzzi and Sansò, 2000, 2004; Kelletat and Schellmann, 2002; Morhange et al., 2006; Scheffers and Scheffers, 2007; Scicchitano et al., 2007; Scheffers et al.,

* Corresponding author. Tel.: +33 442 97 17 91.
E-mail address: mhosseini@cerege.fr (M. Shah-hosseini).

0025-3227/$ – see front matter © 2011 Elsevier B.V. All rights reserved.
doi:10.1016/j.margeo.2011.10.003

2008; Maouche et al., 2009), Japan (Goto et al., 2009, 2010), Australia (Bryant and Nott, 2001), the Caribbean (Scheffers, 2002) and Hawaii (Noormets et al., 2002, 2004; Goff et al., 2006). In numerous studies, boulder deposits have been attributed to tsunamis, extreme storms or a combination of both, but direct observations of mega-clast transport are relatively scarce (e.g. Noormets et al., 2004; Goto et al., 2009).

In this study, coastal boulder deposits on the Makran coast are documented for the first time. Calcareous boulder deposits are observed on rocky coasts at sites between Chabahar port and Lipar lagoon, characterized by angular shapes reworked from the supratidal and intertidal zones with marine bio-erosion features. Using the morphometry and chronology of the mega-clasts, the aim of this paper is to evaluate the characteristics and origin of the waves responsible for the transportation of the boulders by estimating: (i) the minimum wave height capable of transporting the boulders; and (ii) the inland inundation of waves. We compare and contrast our results with measured data from recorded historical events and numerical models.

2. Setting

2.1. Geology, geomorphology and climate

Makran is part of the coastal territory of Iran and Pakistan and stretches for ~1000 km from the Strait of Hormoz, in the south of Iran, to near Karachi in Pakistan. The Makran coast is part of the accretionary wedge of the Makran subduction zone formed by the subduction of the Arabian plate under the Eurasian plate (Byrne et al., 1992; Regard et al., 2005) (Fig. 1). The convergence rate along the subduction zone varies between 2.3 cm/y at the western end and 2.9 cm/y on the eastern margin (Regard et al., 2005). The coast of Makran is marked by a series of prominent headlands separated by bays. Further inland, uplifted Plio-Pleistocene marine marls and sandstones are undergoing intensive erosion. The Holocene coastal uplift rate varies between 0.1 and 0.6 m/ka along the coast, related to episodic uplift in coastal fault blocks (Page et al., 1979; Reyss et al., 1998; Prins et al., 2000). The coastline has been prograding since the mid-Holocene owing to both slight uplift and marine and alluvial sedimentation (Reyss et al., 1998).

The Iranian coast of Makran is a subtropical arid region. Mean annual rainfall is <100 mm and the rainfall variability is extremely high. There are no perennial streams. The tidal range is generally between 2 and 4 m. Winds and currents are in accordance with the monsoon circulation (Fig. 2). The NE monsoon, with moderate winds, begins in October with a maximum intensity in December and January. The SW monsoon is longer and more intense, and therefore has a stronger influence on the wave climate. It begins in April and is at its maximum strength from June to September. Tropical storms and cyclones from the Indian Ocean occasionally occur during May to June (Arz et al., 2003).

2.2. High-energy events in Makran

2.2.1. Large earthquakes and tsunamis

The Makran subduction zone is a major seismic source in the Indian Ocean which has caused numerous earthquakes. Some of the large earthquakes have triggered tsunamis (Quittmeyer and Jacob, 1979; Ambraseys and Melville, 1982; Byrne et al., 1992; Rastogi and Jaiswal, 2006; Dominey-Howes et al., 2007) (Table 1). The last event was the earthquake and tsunami of 1945, which caused heavy loss of life and damage to the coast of Pakistan, Iran and Oman (Ambraseys and Melville, 1982; Pararas-Carayannis, 2006a). Nonetheless, the historical record is relatively poor and incomplete due to the low population density and weak communication with urban centers (Ambraseys and Melville, 1982). Non-seismic events such as large submarine landslides are also able to generate tsunamis (Bourgeois, 2009). Because the submarine morphology of the Makran continental shelf and slope contains very thick sediments, steep slopes and deep canyons (Kopp et al., 2000) an earthquake can potentially trigger tsunamigenic submarine landslides like those reported in the 1945 event (Ambraseys and Melville, 1982). This magnitude 8 to 8.3 earthquake happened off Pakistan near the coastal town of Pasni, with a maximum tsunami wave run-up of 11 to 13 m (Page

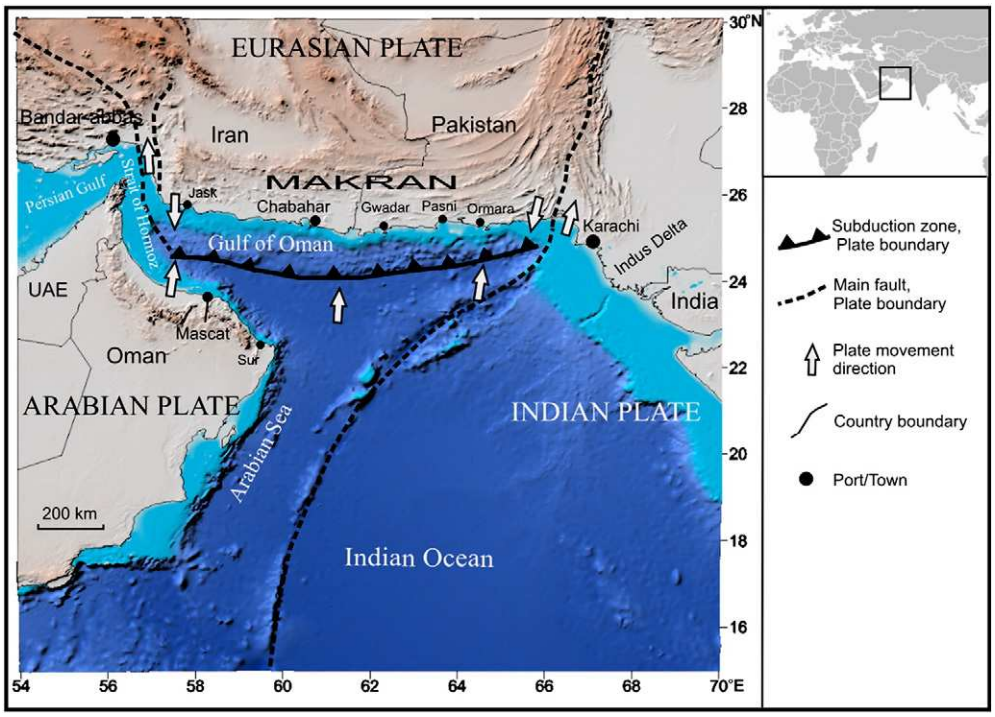

Fig. 1. Tectonic setting of Makran in the northern Indian Ocean.

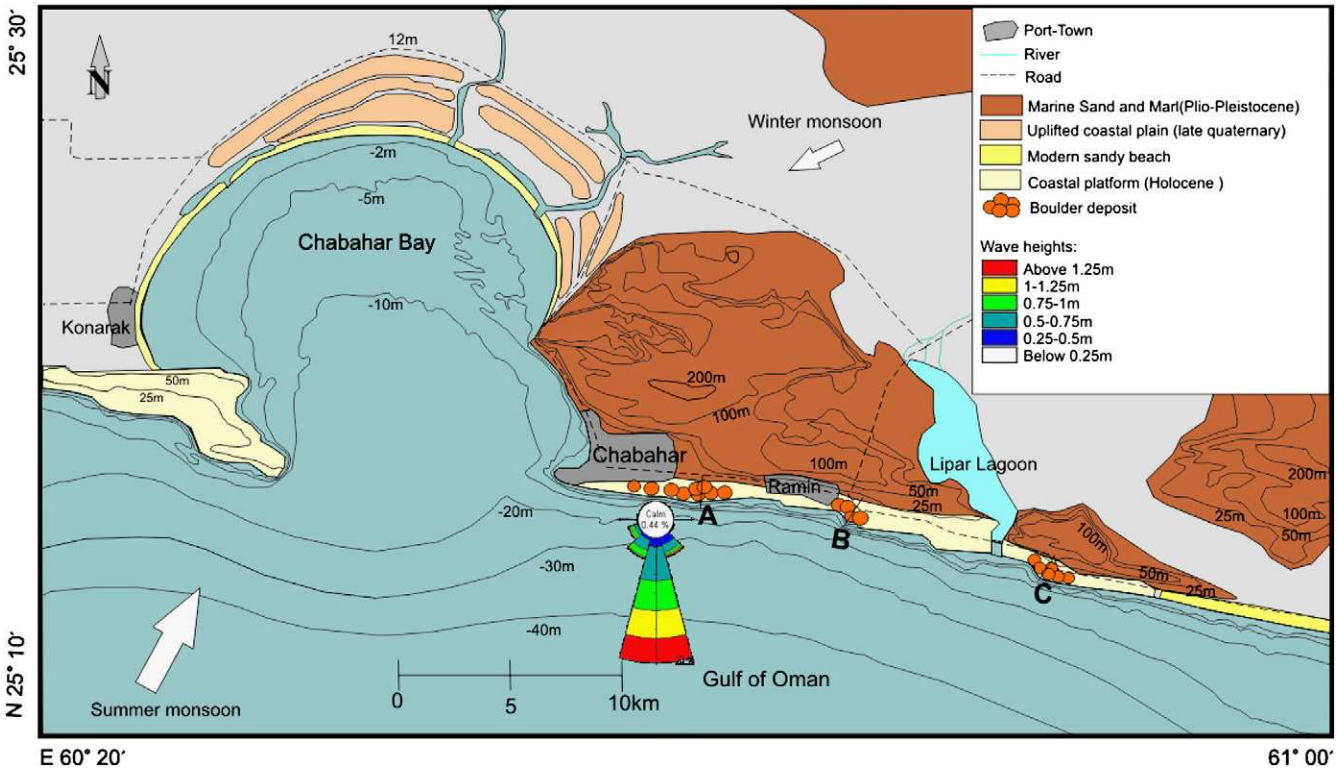

Fig. 2. Location map and climatic features in the study area. Wave heights and directions (1992 to 2002) from the Iranian Sea Wave Model (Chegini et al., 2004).

et al., 1979; Ambraseys and Melville, 1982; Murty and Bapat, 1999; Pararas-Carayannis, 2006a; Rastogi and Jaiswal, 2006). The tsunami waves destroyed fishing villages and caused great damage to the towns of Pasni and Ormara. The earthquake and tsunami claimed 4000 lives (Heck, 1947; Pararas-Carayannis, 2006a). The rupture of submarine telegraph cables suggests that the earthquake may have triggered a delayed underwater landslide (Ambraseys and Melville, 1982). On the Iranian coast, the tsunami waves caused flooding in low lying coastal areas and caused considerable damage (Ambraseys and Melville, 1982; Pararas-Carayannis, 2006a).

Table 1
List of large earthquakes and tsunamis around the Makran subduction zone as attested in historical records.

Year	Location	Remarks	References
326 BC	Eastern Makran near the Indus Delta	Destruction of a Macedonian fleet in Western India by huge waves is described in Greek and Indian historical records.	Murty and Bapat, 1999; Pararas-Carayannis, 2006b; Rastogi and Jaiswal, 2006.
1008 AD	Western Makran, near the strait of Hormoz	An earthquake and tsunami on the southern coast of Iran.	Ambraseys and Melville, 1982.
1483 AD	Western Makran, near the strait of Hormoz	Destructive earthquake in the strait of Hormoz, northwestern Oman was affected by the earthquake.	Quittmeyer and Jacob, 1979; Ambraseys and Melville, 1982.
1765 AD	Eastern Makran	A strong earthquake in the eastern Makran.	Quittmeyer and Jacob, 1979; Byrne et al., 1992.
1851–1864 AD	Middle part of Makran, Near Gwadar	Two great earthquakes in the middle part of Makran affected the town of Gwadar	Quittmeyer and Jacob, 1979; Byrne et al., 1992.
1945 AD	Offshore Pakistani coast near Pasni	Magnitude 8 to 8.3 tsunami wave run-up was 11 to 13 m in the near coast, claimed about 4000 lives.	Quittmeyer and Jacob, 1979; Ambraseys and Melville, 1982; Pararas-Carayannis, 2006a.

2.2.2. Extreme storms

The Iranian coast of Makran receives Indian Ocean swell mostly during the summer monsoon but tropical storms rarely reach the coast. In general, the cyclones tend to travel either west towards Oman or track north to strike Pakistan or India (Fig. 3). Cyclone Gonu, in June 2007, was the most intense tropical storm recorded in the Gulf of Oman and on the Iranian coast. It had an unusual pathway in the Indian Ocean. Gonu is the only category 5 tropical storm to have been recorded in the northwestern Indian Ocean, with maximum wind speed of 142 knots (263 km/h) (Knapp et al., 2010). On the Iranian coast, maximum wind speed of 31 knots (58 km/h) and significant wave height of ~4.5 m were recorded off Chabahar port (depth of 30 m) during Gonu (Golshani and Taebi, 2008; Dibajnia et al., 2010). Gonu caused heavy damage and some loss of life on the coast of Oman and Iran. During fieldwork (2008) we observed watermarks up to 4 m from mean sea level in mud flats of Chabahar Bay. Inundation height of up to 5 m is attested on the Omani coast (Fritz et al., 2010).

3. Methods

3.1. Field methods

During fieldwork, we made direct observations of 58 boulders consisting of measurements of the long, medium and short axes (a, b and c respectively), elevation above mean sea level (according to the intertidal wave cut notch) and inland distance. To accommodate for irregularities in the shape of boulders the mean length of axes are considered. The unit mass of the biogenic calcarenite was determined, using the volumetric method, to be 2.2 g/cm^3 for all boulders. The profiles of three representative boulders bearing coastal platforms were drawn by direct measurement. The origin and setting of boulders prior to transport were investigated using geomorphic features and bioindicators.

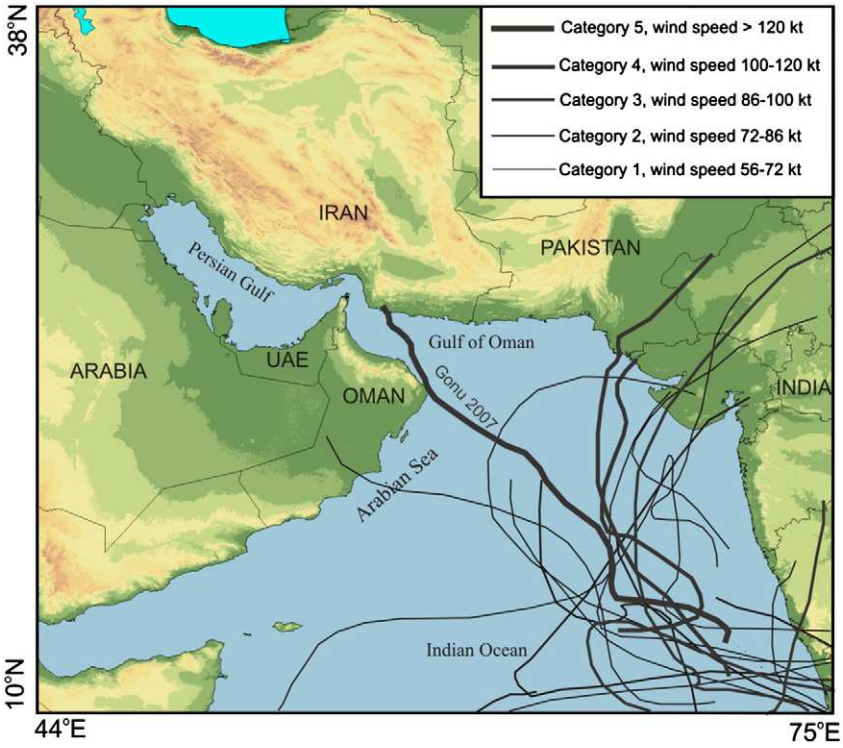

Fig. 3. Tracks of northern Indian Ocean tropical storms with wind speed higher than 56 knots (104 km/h) from 1900 to 2009. Data from the IBTrACS database (Knapp et al., 2010). Cyclone Gonu (2007) is the only recorded category 5 storm in the Gulf of Oman.

In order to estimate the age of boulder deposits, radiocarbon dates were obtained for marine shells *Martezia striata,* collected from three different boulders east of Chabahar. Radiocarbon ages were calibrated using the program Calib.5.0.2 (Stuiver et al., 2005). We applied a marine reservoir age of $\Delta R = 190 \pm 25$ y, determined for the Arabian Sea by radiocarbon dating of pre-bomb shells of a known age (Southon et al., 2002). Radiocarbon is considered as one the best dating methods, Nonetheless, it is important to stress that some factors like death of the organism before transportation or multiple displacements of the boulders can affect the accuracy of dates.

3.2. Boulder transport models

In order to evaluate the wave characteristics responsible for the boulder deposits, we applied boulder transport models adapted to the geomorphological context. Two approaches were followed in order to: (i) evaluate the minimum wave height capable of dislodging and transporting the boulders; and (ii) estimate the inundation distance of the waves. We compared the results with wave height and inundation distances for observed and modeled Makran tsunamis (Heidarzadeh et al., 2009) and storms (Dibajnia et al., 2010).

3.2.1. Minimum wave height required for boulder transport

A wave must have specific hydrodynamic properties to be able to dislodge and transport boulders. These are mainly related to the setting before transport and boulder dimensions. Boulder transport models have been discussed in several studies (e.g. Nott, 1997, 2003; Noormets et al., 2004; Imamura et al., 2008). In a pioneer work, Nott (1997, 2003) has developed hydrological equations to calculate the minimum wave height capable of initiating boulder movement. These equations incorporate the boulder's dimensions, including the long, medium and short axis, boulder and water density, coefficient of drag, coefficient of lift, coefficient of mass, gravitational constant and instantaneous flow acceleration. Nott's equations consider three possible pre-transport settings: submerged, subaerial and joint-bounded (see Nott, 2003). Simplified boulder transport equations for storm and tsunami waves are as follows.

Submerged boulder pre-setting:

$$H_t \geq [0.5a(\rho_s - \rho_w/\rho_w)] / \left[C_D\left(ac/b^2\right) + C_L\right] \quad (1)$$

$$H_s \geq [2a(\rho_s - \rho_w/\rho_w)] / \left[C_D\left(ac/b^2\right) + C_L\right] \quad (2)$$

Subaerial boulder pre-setting:

$$H_t \geq \left[0.25(\rho_s - \rho_w/\rho_w)[(2a - C_M(a/b)(\ /g)]\right] / \left[C_D\left(ac/b^2\right) + C_L\right] \quad (3)$$

$$H_s \geq \left[(\rho_s - \rho_w/\rho_w)[(2a - 4C_M(a/b)(\ /g)]\right] / \left[C_D\left(ac/b^2\right) + C_L\right] \quad (4)$$

Joint-bound boulder pre-setting:

$$H_t \geq [0.25a(\rho_s - \rho_w/\rho_w)]/C_L \quad (5)$$

$$H_s \geq [a(\rho_s - \rho_w/\rho_w)]/C_L \quad (6)$$

where H_t is the tsunami wave height and H_s is the storm wave height at breaking point. a, b and c are the boulder axes lengths; ρ_w is the sea water density; ρ_s is the boulder's density; C_D is the coefficient of drag = 2; C_L is the coefficient of lift = 0.178; C_M is the coefficient of mass = 1; ü is the flow acceleration = 1 m/s^2; g is gravitational acceleration = 9.81 m/s^2.

According to Nott's equations, tsunami waves are four times more capable of transporting boulders compared to storm waves, due to their longer wave period. Wave transport capacities are also strongly influenced by the boulder shape. For instance, the wave height necessary to transport angular shaped boulders is higher than for spherical boulders, planar rectangular boulders require even greater wave height

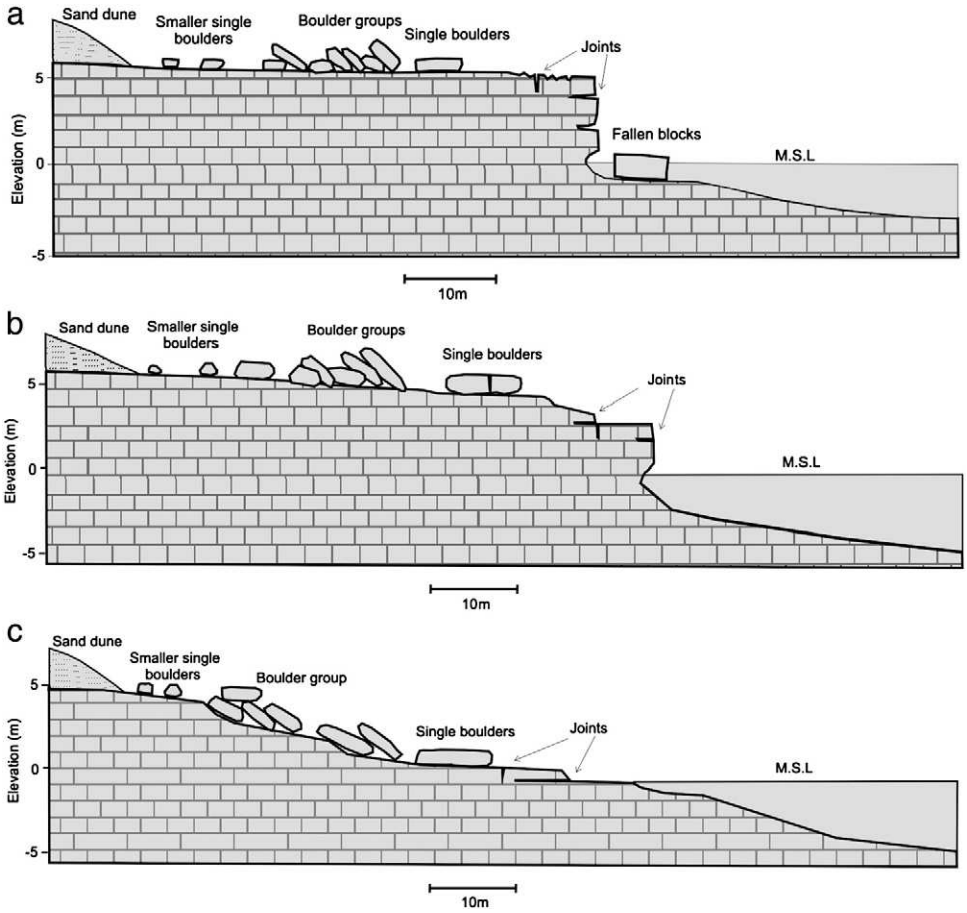

Fig. 4. Schematic coastal profiles of boulder sites, (a) East of Chabahar, (b) East of Ramin, and (c) East of Lipar Lagoon.

to be transported (Nott, 2003). Nott's equations have frequently been applied to evaluate the wave height responsible for boulder transport (e.g. Mastronuzzi et al., 2007; Scicchitano et al., 2007; Maouche et al., 2009; Barbano et al., 2010). However, the accuracy of the model has been debated in some recent works (e.g. Pignatelli et al., 2009; Benner et al., 2010; Switzer and Burston, 2010; Nandasena et al., 2011). Some authors have tried to modify the equations to fit different case studies. For example, in Nott's Joint Bounded Boulder Transport (JBBT) scenario, it is assumed that prior to transport the boulder is limited by five sides in the coastal cliff (the four sides and the undersurface of the rock). The upper side is the only surface that the wave can act on, while in many studied cases one of the block's sides is directly facing the wave action due to the rectangular joints on the edge of the coastal cliff. Nott's tsunami equations have been modified to accommodate this pre-setting as follows (Pignatelli et al., 2009):

$$H_t \geq [0.5c(\rho_S - \rho_w/\rho_w)]/C_L \quad (7)$$

We used the same approach to modify Nott's joint bounded equations for storm waves when the boulders' thickness is directly exposed to wave impact:

$$H_S \geq [2c(\rho_S - \rho_w/\rho_w)]/C_L \quad (8)$$

According to Benner et al. (2010), the length of the lever arm and acceleration of the water around subaerial boulders is neglected in Nott's equations. They also noted that the coefficient of lift is 1 for cuboid and 2 for prismatic boulders. Benner et al. (2010) have suggested the following corrections be applied to the subaerial boulder transport equations:

$$H_t \geq \left[0.5bc\left[b(\rho_s - \rho_w)/\rho_w - \rho_s C_m\ c/(\rho_w g)\right]/C_D c^2 + C_L b^2\right] \quad (9)$$

$$H_s \geq \left[2bc\left[b(\rho_s - \rho_w)/\rho_w - \rho_s C_m\ c/(\rho_w g)\right]/C_D c^2 + C_L b^2\right] \quad (10)$$

3.2.2. Inundation distance

The inland position of boulders has been used to evaluate the wave characteristics responsible for their transport (Noormets et al., 2004; Goto et al., 2007; Imamura et al., 2008). The mechanism of transport has an important role in dictating the final position of the boulders. Noormets et al. (2004) consider sliding as a common mechanism of transport for large and irregular boulders, while smaller and platy boulders are usually found in overturned positions, which suggest rolling. Goto et al. (2007) suggest saltation for the boulders observed after the 2004 Indian Ocean tsunami. Imamura et al. (2008) have performed experiments for boulder transport in an open channel. They have reported that cubic or rectangular boulders are mostly transported by rolling or saltation. According to Noormet's model (2004), the final distance of a boulder is equal to the minimum bore height required to move the boulder on the coastal platform. Assuming sliding as the main transport mechanism, a boulder stops moving when

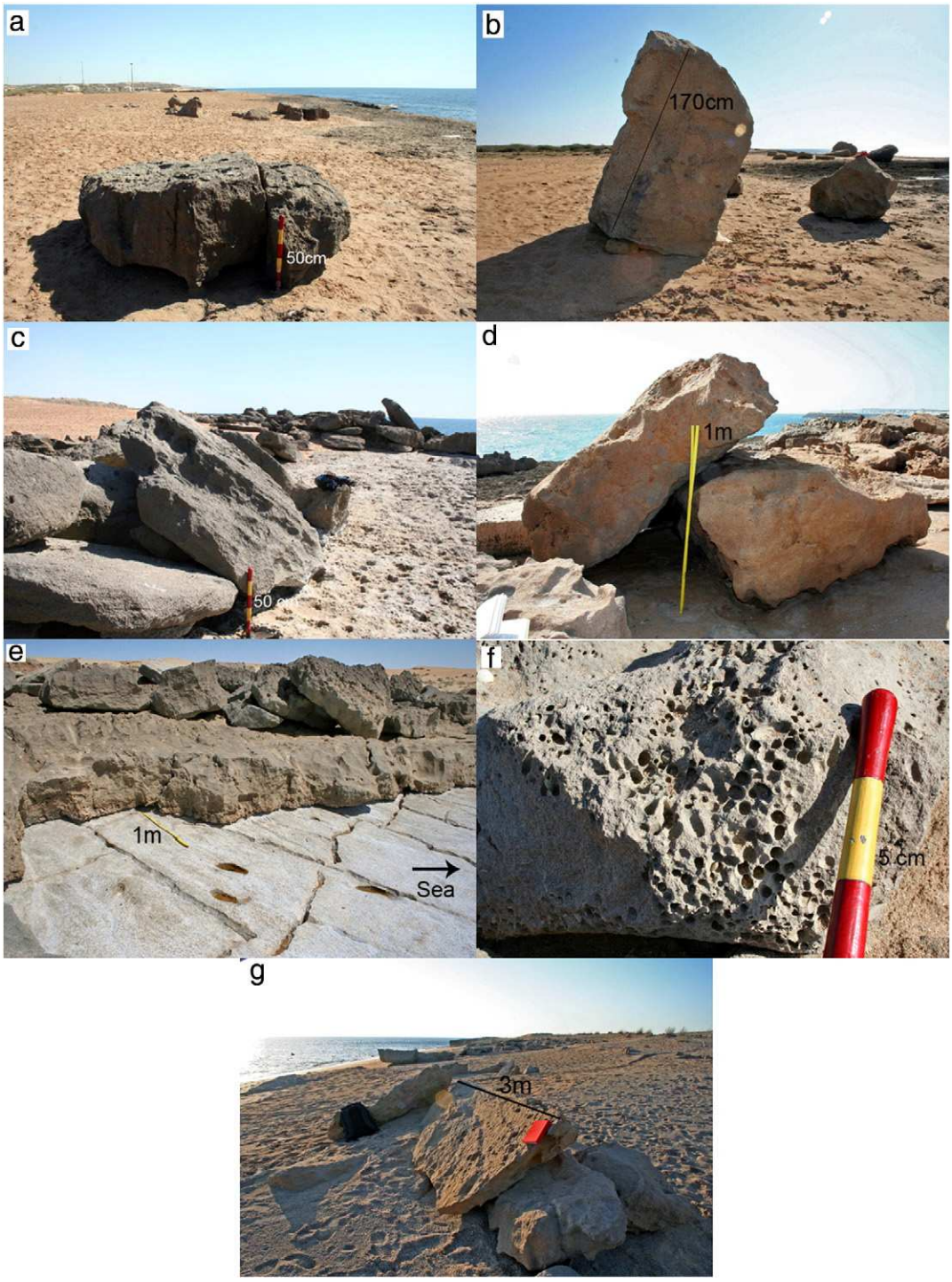

Fig. 5. (a) Single fractured boulder east of Chabahar. (b) Standing boulder, east of Chabahar. (c) Boulder groups east of Chabahar. (d) Over-turned boulder south of Ramin, the erosional surface feature is found at the base of the boulder. (e) Rectangular joints on the coastal platform, east of Ramin, the size and shape of the boulders correspond to the fracture system. (f) Boreholes of the marine bivalve *Martezia striata* found on some boulders. (g) Platy boulder east of Lipar.

the force of fluid drag is equal or smaller than the force of friction between the boulder and the surface:

$$F_D \leq F_\mu \tag{11}$$

The force of drag and friction can be calculated as follows (Noormets et al., 2004):

$$\text{Force of drag} : F_D = 0.5\rho_w C_D(ac)v^2 \tag{12}$$

ρ_w is water density; C_D is coefficient of drag = 1.95; a and c are the long and short axes of the boulder and v is flow velocity.

$$\text{Force of friction} : F_\mu = \mu mg \tag{13}$$

μ is the coefficient of friction = 0.7; m is the mass and g is gravitational acceleration.

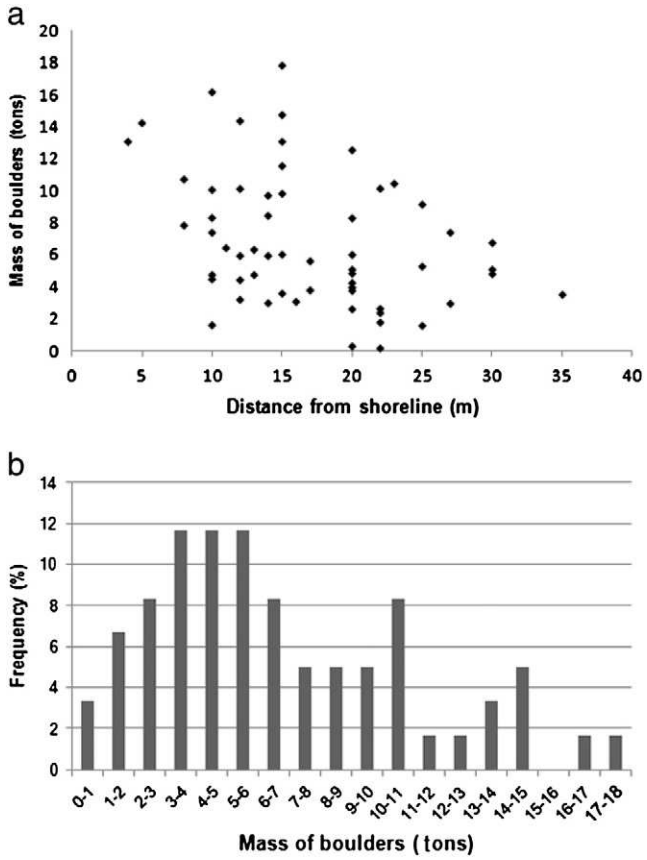

Fig. 6. (a) Distance from shoreline vs. boulder weight for all the measured boulders, a landward fining trend is recognizable. (b) Boulders weight vs. frequency, the peak 3–6 t is of note.

The flow velocity and wave height at the coastline are related as follows (Fukui et al., 1963):

$$v^2 = \delta g h \tag{14}$$

v is the flow velocity, g is the gravitational acceleration and h is the wave height, δ is a constant describing the wave typology derived from empirical relations (Fukui et al., 1963).

By combining Eqs. (11) to (14), the storm and tsunami wave heights at final inland position of boulders can be calculated (Barbano et al., 2010).

$$\text{Storm}: H_{sf} = [2\mu\rho_s abc]/(C_D\rho_w ac) \tag{15}$$

$$\text{Tsunami}: H_{tf} = [0.5\mu\rho_s abc]/(C_D\rho_w ac) \tag{16}$$

A wave's height at a given distance over the platform is related to the wave's initial height at the cliff's edge and its period as follows (Cox and Machemehl, 1986; Noormets et al., 2004):

$$h = \left[\sqrt{(R-E)} - (5Xi/T\sqrt{g})\right]^2 \tag{17}$$

where h is the bore's depth at the boulder's inland distance (Xi); R is wave height at the breaking point; and E is the platform elevation (the term R–E is the portion of bore above the platform surface).

By including the slope of a coastal platform (α) considering (X = Xmax/cos α), the maximum inland inundation of a wave could be obtained from Eq. (17) as follows (Barbano et al., 2010):

$$X_{max} = \left[(T\sqrt{g})\sqrt{(R-E)}\cos\alpha\right]/5 \tag{18}$$

As expected, the maximum inland inundation of tsunamis or storms is greater than the final distance of mega-clasts.

3.2.3. Wave height at breaking point

To calculate the wave height and inundation for boulder transport, the wave height at breaking point is needed. While in many cases the available data are recorded offshore, to convert offshore wave height to breaker we apply the Sunamura and Horikawa (1974) equation. It takes into account fundamental parameters, such as the wave steepness (H/L) and the seafloor slope (tanβ):

$$Hb = [(\tan\beta)\ 0.2(Ho/Lo) - 0.25]Ho \tag{19}$$

Where Hb is the breaking wave height, tanβ is the slope between the shoreline to −10 m depth, Ho and Lo are respectively the wave height and length in deep water ($Lo = 1.56\,T^2$).

In order to include the wave refraction processes between the offshore and the nearshore, we substitute the deep water wave height (Ho in the original equation of Sunamura and Horikawa, 1974) with the nearshore wave height (H'o), before the breaking point, at around 15 m depth (shoaling and the friction processes are neglected).

$$H'o = Ho.Kr \tag{20}$$

where Ho is the wave height in the deepwater and Kr is the coefficient of refraction estimated by using the linear wave theory.

4. Results

4.1. Boulder deposits

The studied boulders are mostly concentrated at three locations along the rocky coast: (i) east of Chabahar, (ii) east of Ramin and (iii) east of Lipar Lagoon (Fig. 2). Boulders were found as single elements or in groups. The boulder groups are sometimes arranged as imbricated clusters forming ridges along the coastline. They usually show rectangular forms and sometimes prismatic shapes, with clearly broken edges. At each location, tens to hundreds of boulders could be found. Boulders are scattered on a coastal strip, whose precise inward extension appears to be obscured by sand dunes. The volume of the boulders is up to 8 m^3. Morphological features such as supratidal karstic forms on the surface of the boulders and their rectangular shapes coincide with the joints and morphology of the platform. This suggests that most of them have been carved out of the cliff edge. The presence of the marine boring bivalve *Martezia striata* is consistent with a subtidal origin for some of the boulders (<10%). Plotting the mass of the boulders against their distance from the shoreline shows a landward fining trend. Most of the large boulders could be found between 10 and 20 m from the edge of the coast (Fig. 6a). Boulders are generally between 2 and 6 t in weight (Fig. 6b).

4.1.1. East of Chabahar

In an area about 1.5 km along the coast of Chabahar, the major Iranian port in the Gulf of Oman, boulder deposits are found on a gently sloping coastal platform, which ends in a wave-cut cliff on the seaward side (Fig. 4a). The elevation of the coastal platform varies from ~2 m above sea level in the eastern part to ~6 m at the western end, where only single boulders are found. Some of the boulders are in an unstable position or fractured into two or three parts (Fig. 5a and b). Boulders are more abundant in the eastern part and form groups (Fig. 5c). The largest measured boulder had a volume of ~8 m^3 and weighs ~18 t. Most of the boulders show a planar shape and marine bivalve boreholes and shells are observed on some of them (Fig. 5f).

Table 2
Boulder morphometric properties and calculated minimum tsunami (Ht) and storm (Hs) wave heights capable of carving and transporting them in the JBBT model. Wave height results from Nott's original equations and modified equations by Pignatelli et al., 2009 are compared.

Boulder	Axis (m)			Distance (m)	Elevation (m)	Volume (m^3)	Weight (t)	Ht (m) (Nott, 2003)	Hs (m) (Nott, 2003)	Ht (m) Pignatelli et al., 2009	Hs (m) Pignatelli et al., 2009
	a	b	c								
East of Chabahar											
CH01	2.3	1.5	0.5	17	5	1.73	3.80	3.76	15.05	1.6	6.4
CH02	2.5	1.8	0.65	11	5	2.93	6.44	4.09	16.36	2.1	8.3
CH03	2.5	1.2	0.8	25	4	2.40	5.28	4.09	16.36	2.6	10.2
CH04	1.5	1.5	1.2	14	4	2.70	5.94	2.45	9.82	3.8	15.3
CH05	2.6	1.6	1.1	10	5	4.58	10.07	4.25	17.02	3.5	14.0
CH06	1.7	1	0.8	14	5	1.36	2.99	2.78	11.13	2.6	10.2
CH07	1.7	2	0.6	10	5	2.04	4.49	2.78	11.13	1.9	7.7
CH08	2.1	1.3	0.8	30	5	2.18	4.80	3.44	13.74	2.6	10.2
CH11	2.5	0.8	0.6	22	5	1.20	2.64	4.09	16.36	1.9	7.7
CH12	0.5	0.5	0.3	22	5	0.08	0.17	0.82	3.27	1.9	7.7
CH13	3.5	1.6	0.6	27	4	3.36	7.39	5.73	22.91	1.9	7.7
CH14	2.4	2	0.7	27	4	1.34	2.96	3.93	15.71	2.2	8.9
CH15	2	1.5	0.6	20	5	1.80	3.96	3.27	13.09	1.9	7.7
CH16	1.7	1	0.7	20	5	1.19	2.62	2.78	11.13	2.2	8.9
CH17	2.3	1.4	0.6	20	5	1.93	4.25	3.76	15.05	1.9	7.7
CH18	2.2	1.5	0.7	20	5	2.31	5.08	3.60	14.40	2.2	8.9
CH19	1.9	1.5	0.6	20	5	1.71	3.76	3.11	12.44	1.9	7.7
CH20	0.85	0.4	0.4	20	5	0.14	0.30	1.39	5.56	1.3	5.1
CH21	2.6	2.9	0.5	20	2.5	3.77	8.29	4.25	17.02	1.6	6.4
CH22	1.5	0.9	0.6	22	3	0.81	1.78	2.45	9.82	1.9	7.7
CH23	3.2	1.8	0.8	22	2.5	4.61	10.14	5.24	20.94	2.6	10.2
CH24	1.9	1.9	0.3	22	2.5	1.08	2.38	3.11	12.44	1.0	3.8
CH25	2.9	2.8	0.6	8	3	4.87	10.72	4.75	18.98	1.9	7.7
CH26	2	1.8	0.6	13	3.5	2.16	4.75	3.27	13.09	1.9	7.7
CH27	3.4	1.5	0.5	17	2.5	2.55	5.61	5.56	22.25	1.6	6.4
CH28	4.5	3	0.6	15	3	8.10	17.82	7.36	29.45	1.9	7.7
East of Ramin											
BR01	1.5	1.4	0.35	10	6	0.74	1.62	2.45	9.82	1.1	4.5
BR02	3.3	2	0.9	4	6	5.94	13.07	5.40	21.60	2.9	11.5
BR03	3.1	2.4	0.6	15	6	4.46	9.82	5.07	20.29	1.9	7.7
Br04	3.4	2.4	0.9	10	6	7.34	16.16	5.56	22.25	2.9	11.5
BR05	2.3	2.5	0.5	13	6	2.88	6.33	3.76	15.05	1.6	6.4
BR06	1.7	1.6	0.6	15	6	1.63	3.59	2.78	11.13	1.9	7.7
BR07	2.2	2	0.5	20	5	2.20	4.84	3.60	14.40	1.6	6.4
BR08	4.2	2.2	0.7	5	5	6.47	14.23	6.87	27.49	2.2	8.9
BR09	3	2.5	0.7	15	4	5.25	11.55	4.91	19.64	2.2	8.9
BR10	3.3	3	0.6	15	4	5.94	13.07	5.40	21.60	1.9	7.7
BR11	3.8	2.5	0.6	20	4	5.70	12.54	6.22	24.87	1.9	7.7
BR12	2.5	1.9	1	23	6	4.75	10.45	4.09	16.36	3.2	12.8
BR13	3.3	1.4	0.9	25	6	4.16	9.15	5.40	21.60	2.9	11.5
BR14	3.4	1.6	1.2	12	5	6.53	14.36	5.56	22.25	3.8	15.3
BR15	1.8	1.4	0.8	12	5	2.02	4.44	2.95	11.78	2.6	10.2
BR16	2.5	2.3	0.8	12	5	4.60	10.12	4.09	16.36	2.6	10.2
BR17	2.3	1.7	0.7	15	5	2.74	6.02	3.76	15.05	2.2	8.9
BR18	2.5	1.8	0.6	12	4	2.70	5.94	4.09	16.36	1.9	7.7
BR19	2	1.8	0.6	10	4	2.16	4.75	3.27	13.09	1.9	7.7
BR20	2.6	1.5	0.7	20	5	2.73	6.01	4.25	17.02	2.2	8.9
BR21	1.6	1.3	0.7	12	4	1.46	3.20	2.62	10.47	2.2	8.9
BR22	2.9	2.1	1.1	15	4	6.70	14.74	4.75	18.98	3.5	14.0
BR23	3.5	1.8	0.7	14	4	4.41	9.70	5.73	22.91	2.2	8.9
BR24	3	1.6	0.7	10	3	3.36	7.39	4.91	19.64	2.2	8.9
BR25	3	1.8	0.7	10	3	3.78	8.32	4.91	19.64	2.2	8.9
BR26	1.8	1.8	1.1	8	3	3.56	7.84	2.95	11.78	3.5	14.0
East of Lipar											
L01	4	1.6	0.6	14	2.5	3.84	8.45	1.13	4.54	1.9	7.7
L02	2.5	1.4	0.4	16	2.5	1.40	3.08	1.22	4.86	1.3	5.1
L03	3	1.2	0.2	25	3	0.72	1.58	1.73	6.91	0.6	2.6
L04	3.5	3.3	0.9	30	2.5	3.07	6.75	2.70	10.78	2.9	11.5
L05	3.3	1.4	0.5	30	2.5	2.31	5.08	1.03	4.13	1.6	6.4
L06	2.5	1.6	0.4	35	3	1.60	3.52	1.52	6.07	1.3	5.1

4.1.2. East of Ramin

About 15 km east of Chabahar port, east of Ramin, we investigated another boulder field. In this area, mega-clasts are found on a gently sloping coastal platform elevated 4 to 5 m above sea level (Fig. 4b). The coastal platform has a step-like morphology at the edge of the cliff and shows a rectangular system of joints that is coincident with the forms and sizes of the boulders (Fig. 5e). Boulders are scattered on a coastal strip ~200 m long and ~40 m wide between the sea and sand dunes. They form imbricated groups in some parts. The marine bivalve boreholes were only found on smaller boulders up to 1 m^3 in volume. Larger boulders up to 7.3 m^3 show a rectangular shape and sharp edges. Some boulders are clearly overturned in a way

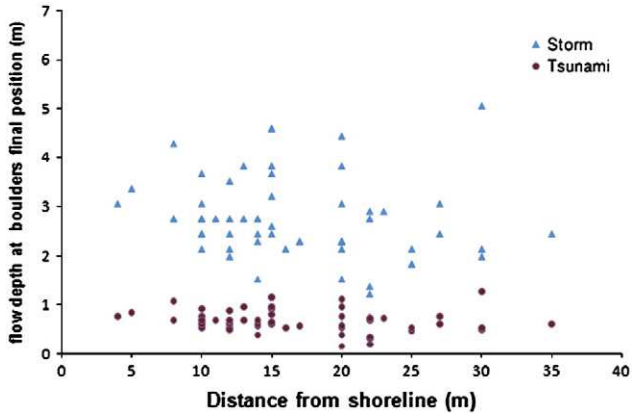

Fig.7. Minimum storm and tsunami flow depth at final boulder positions (Eqs. 15 and 16).

that supratidal karstic features are found on the boulder's base (Fig. 5d).

4.1.3. East of Lipar

Another boulder field is observed ~25 km east of Chabahar Port, near Lipar Lagoon (Fig. 2). Here the coastal platform is lower compared to the other two sections (Fig. 4c). Boulder deposits could be found for ~2 km along the coast. In the eastern part, relatively large single boulders (up to 4 m long with a volume of 3.8 m^3) are more frequent (Fig. 5g), while the western end comprises smaller (<1 m^3) boulders forming ridges along the coast. The largest measured boulder in this section has a volume of 3.8 m^3.

4.2. Evaluating minimum wave height required for boulder transport

In light of the geomorphic context of our study area, we applied the Joint Bound Boulder Transport model to calculate the minimum wave height necessary for boulder detachment and transport. Carved scars on the edge of the coastal platform, along with the rectangular forms and surface erosional features on boulders suggest that most of the boulders are carved out of the rocky cliff. Pignatelli et al.'s (2009) equations are most appropriate for wave height calculations due to similar geomorphic settings. Tsunami and storm wave height have been calculated for measured boulders (Table 2).

4.3. Evaluating wave height at final boulder resting distance

To evaluate the inundation distance of waves, we calculated the flow depth at final position for each boulder (Eqs. 15 and 16). Minimum storm and tsunami flow depths at final position of boulders are plotted in Fig. 7. These results show that tsunami wave heights over the coastal platform are generally >1 m above the blocks (maximum 1.3 m), whereas required storm bore heights are generally >3 m (maximum 5 m).

4.4. Age of boulder deposits

Radiocarbon dating was performed on three *Martezia striata* shells (Table 3). When comparing the ages to the historical records, two age ranges could be related to the event of 1008, reported in southern Iran around the strait of Hormoz (Ambraseys and Melville, 1982). East of Ramin fresh looking broken edges and limited surface solution evoke younger ages for boulder deposits. For more accurate age determination of the boulder deposits, more dating is needed.

5. Discussion

5.1. Wave origin

Transported boulders have been used as indicators of large waves in numerous studies, but direct observations of boulder transportation due to known tsunami or storm events are relatively rare. For example, Noormets et al. (2004) have investigated the transport ability of storms and tsunami waves in Hawaii by comparing aerial photographs of the coastal platform before and after impacts. Goto et al. (2007, 2009) have documented boulder transport by the 2004 Indian Ocean tsunami and tropical storms in the Pacific Ocean. Transportation of cliff top boulders by extreme storms is documented in the north Atlantic (Williams and Hall, 2004; Suanez et al., 2009; Etienne and Paris, 2010). Mega-clast dislodgment is observed during both powerful storms and tsunami events. The main difference in transport capacity of storm and tsunami waves is related to wave periods. Storms are capable of quarrying large boulders from the shoreline but do not usually have sufficient power to displace them inland. By contrast, the long wave of tsunamis is more likely to transport mega-clasts inland due to the longer duration of their action (Noormets et al., 2004). Some recent studies have attempted to define models to distinguish tsunami and storm boulder deposits (e.g. Goto et al., 2010; Lorang, 2010) but, in most cases, ambiguities persist due to the different geological and meteorological contexts of studied sites.

To evaluate the origin of the waves responsible for boulder transport in our study area, we compare calculated tsunami and storm waves to extreme high-energy events recorded on the Makran coast. Due to insufficient historical data, tsunami and storm modeling helped us to estimate the largest probable events. We used the following storm and tsunami numerical models as the largest probable events on the Iranian coast of Makran:

i) Strongest probable storm: Dibajnia et al. (2010) have used three data sources to produce a maximum significant wave height model: (1) IBTrACS (Knapp et al., 2010); (2) the U.S. Navy Joint Typhoon Warning Center's (JTWC); and (3) historic storm tracks from the Indian Meteorological Department. The model yielded significant wave height of up to 8.8 m with a period of 15 s off the Iranian coast near Chabahar.
ii) The worst-case tsunami: Heidarzadeh et al. (2009) have modeled the near field tsunami waves for Makran. By applying the rupture length equal to half the length of the plate boundary (500 km) to the model, the result is tsunami wave height of 6 to 9 m along the coast. We apply wave height of 6 m and a period of 15 min for the study area.

To compare the calculated waves to extreme events two approaches are used: (i) minimum wave height capable of initiating boulder transport; and (ii) inland inundation distance. Offshore storm wave heights are converted to breaker heights using Eqs. (19) and (20).

Table 3
Radiocarbon dating results of the marine boring bivalve *Martezia striata* collected from boulders east of Chabahar. Calibrated dates are reported to 2σ.

Boulder no.	Boulder weight (kg)	$\delta^{13}C$	Radiocarbon age	Calibrated age (year BP)	Mean ΔR for Western Arabian Sea	Corrected age for reservoir effect (year BP)	Corrected age for reservoir effect (calendar years)
CH 01	3800	+3.50	2155 ± 30	1750 ± 45	190 ± 25	1560 ± 51	340–440 AD
CH 02	6440	+1.90	1630 ± 30	1202 ± 40	190 ± 25	1012 ± 47	890–980 AD
CH 22	1780	+2.50	1760 ± 30	1304 ± 30	190 ± 25	1114 ± 39	800–870 AD

Table 4
Maximum inland inundation for known and modeled events on the boulder bearing coastal platform near Chabahar. Maximum uplift of 0.5 m is considered according to age determinations.

Event	Significant offshore wave height (m)	Breaking wave height (m)	Wave period (s)	Platforms elevation (m)	Platforms steepness (Degree)	Maximum inundation (m)
Gonu cyclone (2007)	5	5.4	10	2.5	3	10.7
Modeled strongest storm (Dibajnia et al., 2010)	8.8	9.4	15	2.5	3	24.6
Calculated tsunami based on boulder dimensions (this study)	–	4	900	2.5	3	690
Modeled worst-case tsunami (Heidarzadeh et al., 2009)	–	6	900	2.5	3	1050

5.2. Minimum wave height capable of initiating boulder transport

According to our results (Table 2), the largest boulders could be detached and transported by a tsunami wave of ~4 m (JBBT model, modified by Pignatelli et al., 2009). The minimum required storm wave height is about 15 m. The strongest recorded storm (Gonu) has a significant wave height of <5 m, which can generate a maximum wave height of 5.4 m at breaking point. The strongest modeled storm produces offshore wave height of 8.8 m and can produce a maximum breaker wave height of 9.4 m. We conclude that no known or probable storm would have been strong enough to carve out and transport the largest boulders.

5.3. Maximum inundation of extreme events

The maximum inland inundation of extreme events is estimated by inputting wave heights and periods to Eq. (17), based on the Noormet's model (Barbano et al., 2010). The results are presented in Table 4. The calculated flow depths at final position for each boulder (Fig. 8) are compared with the wave height decay curves of storm and tsunami events from Table 4. We show that the strongest known storm, Gonu, is not able to transport any of the boulders to their final position. This is in agreement with our interviews of local inhabitants after Gonu. The modeled maximum storm is only able to transport some boulders (under the dashed line) to their final position not more than 10 m in distance (Fig. 8). By contrast, a tsunami wave height of 4 m is enough to move all boulders to their final position (Fig. 9).

5.4. Boulder reworking

Boulder transport could result from multiple events. To evaluate the wave heights that are able of remobilizing the boulders we applied subaerial transport models (Eqs. 9 and 10). The calculated wave heights required to remobilize boulders on the coastal platform are plotted against the wave decay curves of extreme events from Table 4, for storms (Fig. 10) and tsunamis (Fig. 11). The wave height required to remobilize boulders is higher than Gonu. The strongest modeled storm waves could only remobilize boulders close to the coastline (<5 m), whereas a tsunami wave of 4 m is able to remobilize most (~90%) of the boulders.

Our data suggest a tsunami source for boulder deposits. The most plausible candidate for generating this tsunami is the near-field Makran subduction zone. Large earthquakes in the eastern part of Makran (e.g. the 1945 event) are reported to have generated tsunami wave run-up heights of more than 11 m near the epicenter and considerable wave run-up along the entire Makran coast (Ambraseys and Melville, 1982; Pararas-Carayannis, 2006a; Rastogi and Jaiswal, 2006). However, this was probably not sufficient to generate enough wave height for boulder deposits in the western part of the Makran. Interviews with elderly inhabitants evoke maximum tsunami wave run-up of 2–3 m in Chabahar after the 1945 event (Naderi and Hamzeh, 2010; E. Okal, personal communication). The geomorphological tsunami evidence implies that the western part of the Makran subduction zone is capable of generating large tsunamigenic earthquakes, though the frequency of events is inferior to the eastern part.

6. Conclusion

Coastal boulder deposits attesting to large waves are documented along the rocky coast of Makran, from Chabahar to Lipar. The coastal wave height required to initiate boulder transport and wave heights at final position were compared to wave height decay curves for known and modeled storms and tsunamis. According to our results no known storm event is able to detach and transport the studied boulders. The strongest modeled storm is able to detach and

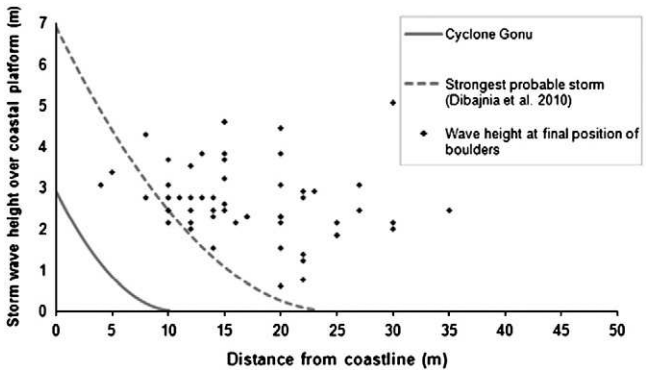

Fig. 8. Storm wave height for each boulder at final distance compared to known (Gonu) and modeled storm wave height decay curves.

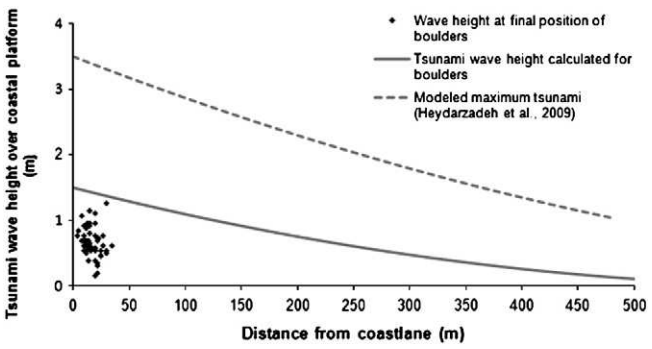

Fig. 9. Tsunami wave height for each boulder at final distance compared to calculated and modeled tsunami wave height decay curves.

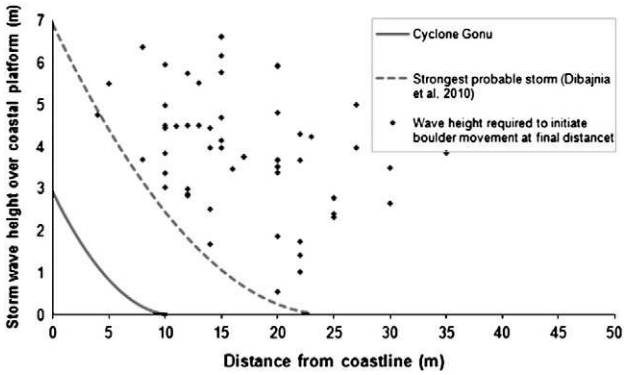

Fig. 10. Storm wave height required to initiate boulder movement at final inland distance compared to known (Gonu) and modeled storm wave height decay curves.

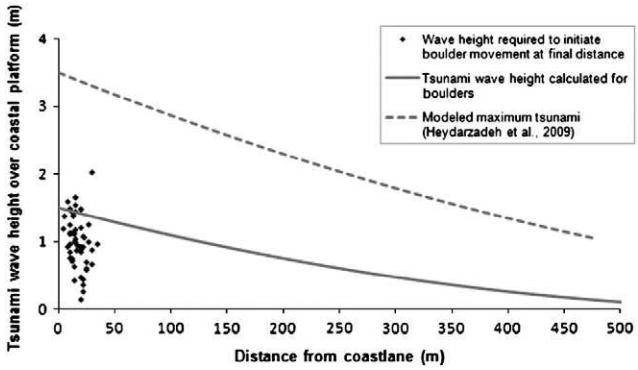

Fig. 11. Tsunami wave height required to initiate boulder movement at final inland distance compared to tsunami wave height calculated for boulders and modeled maximum tsunami wave height decay curves.

transport some boulders near the coastline (up to 10 m inland), but is not strong enough to transport the larger boulders. Controversially, tsunami waves with coastal height of 4 m can explain the boulder deposits. Large near-field earthquakes in the Makran Subduction zone are able to generate tsunami wave run-up to explain the boulder transport. Radiocarbon dating of marine boring bivalves yielded ages spanning 340 to 980 AD. Two age ranges could be related to the historical earthquake and tsunami of 1008 AD, around the Strait of Hormoz.

Geomorphological tsunami evidence implies that the western part of the Makran subduction zone is capable of generating large tsunamigenic earthquakes. This can improve our knowledge of paleotsunami and coastal hazards along the poorly studied Makran coast. The research also contributes to the Indian Ocean's coastal hazard database to assess and mitigate against future catastrophes. Along with coastal geomorphological researches all over the world, this study can improve the knowledge of hydrology of large waves and their impact on the rocky coast.

Acknowledgments

This study is a result of cooperation between European center of geoscience and environmental researches (CEREGE) and Iranian national institute for oceanography (INIO) and was financially supported by the Franco–Iranian research program of PHC Gundishapur (project no. 23178UD) offered by Egide, French Ministry of Foreign and European Affairs and Iranian Center for International Scientific Studies and collaborations (CISSC). Radiocarbon dating was supported by ARTEMIS INSU. We wish to thank Brian Atwater, Giuseppe Mastronuzzi, Dieter Kelletat and an anonymous reviewer for their constructive comments.

References

Ambraseys, N.N., Melville, C.P., 1982. A History of Persian Earthquakes. Cambridge University Press, Cambridge. 219 pp.
Arz, H.W., Lamy, F., Patzold, J., Muller, P.J., Prins, M., 2003. Mediterranean moisture source for an early-Holocene humid period in the northern Red Sea. Science 300, 118–121.
Barbano, M.S., Pirrotta, C., Gerardi, F., 2010. Large boulders along the south-eastern Ionian coast of Sicily: storm or tsunami deposits? Marine Geology 275, 140–154.
Benner, R., Browne, T., Brückner, H., Kelletat, D., Scheffers, A., 2010. Boulder transport by waves: progress in physical modeling. Zeitschrift für Geomorphologie 54 (3), 127–146.
Bourgeois, J., 2009. The geologic effects and records of tsunamis. In: Bernard, E.N., Robinson, A.R. (Eds.), Tsunamis. The Sea, Volume 15. Harvard University Press, Cambridge, Massachusetts, pp. 55–91.
Bryant, E.A., Nott, J.F., 2001. Geological indicators of large tsunami in Australia. Natural Hazards 24, 231–249.
Byrne, D.E., Sykes, L.R., Davis, D.M., 1992. Great thrust earthquakes and aseismic slip along the plate boundary of the Makran Subduction Zone. Journal of Geophysical Research 97, 449–478.
Chegini, V., Goilshani, A., Taebi, S., 2004. Iranian Sea Wave Modelling (ISWM), Phase 3: Persian Gulf and Sea of Oman. Iranian National Institute for Oceanography (INIO), Technical Report for the Ports and Maritime Organization (PSO) of Iran. 455 pp.
Cox, J.C., Machemehl, J., 1986. Overland bore propagation due to overtopping wave. Journal of Waterway, Port, Coastal, and Ocean Engineering 112, 161–163.
Dibajnia, M., Soltanpour, M., Nairn, R., Allahyar, M., 2010. In: Charabi, Y. (Ed.), Indian Ocean Tropical Cyclones and Climate Change. Springer. 373 pp.
Dominey-Howes, D., Cummins, P., Burbidge, D., 2007. Historic records of teletsunami in the Indian Ocean and insights from numerical modelling. Natural Hazards 42, 1–17.
Donato, S.V., Reinhardt, E.G., Boyce, J.I., Rothaus, R., Vosmer, T., 2008. Identifying tsunami deposits using bivalve shell taphonomy. Geology 36, 199–202.
Donato, S.V., Reinhardt, E.G., Boyce, J.I., Pilarczyk, J.E., Jupp, B.P., 2009. Particle-size distribution of inferred tsunami deposits in Sur Lagoon, Sultanate of Oman. Marine Geology 257, 54–64.
Etienne, S., Paris, R., 2010. Boulder accumulations related to storms on the south coast of the Reykjanes Peninsula (Iceland). Geomorphology 114, 55–70.
Fritz, H.M., Blount, C.D., Albusaidi, F.B., Al-Harthy, A.H.M., 2010. Cyclone Gonu storm surge in Oman. Estuarine, Coastal and Shelf Science 86, 102–106.
Fukui, Y., Nakamura, M., Shiraishi, H., Sasaki, Y., 1963. Hydraulic Study on Tsunami. Coastal Engineering in Japan, The Japan Society of Civil Engineers, Tokyo 6, 67–82.
Geist, E., Titov, V., Synolakis, C., 2006. Tsunami: wave of change. Scientific American 294 (1), 56–63.
Goff, J., Dudley, W.C., de Maintenon, M.J., Cain, G., Coney, J.P., 2006. The largest local tsunami in 20th century Hawaii. Marine Geology 226, 65–79.
Golshani, A., Taebi, S., 2008. Numerical modeling and warning procedures for Gonu Super Cyclone along Iranian Coastlines. In: Wallendorf, L., et al. (Ed.), Proceedings of the Third COPRI Solutions to Coastal Disasters Conference. ASCE, Oahu, HI. 13–16 April 2008.
Goto, K., Chavanich, S.A., Imamura, F., Kunthasap, P., Matsui, T., Minoura, K., Sugawara, D., Yanagisawa, H., 2007. Distribution, origin and transport process of boulders deposited by the 2004 Indian Ocean tsunami at Pakarang Cape, Thailand. Sedimentary Geology 202, 821–837.
Goto, K., Okada, K., Imamura, F., 2009. Characteristics and hydrodynamics of boulders transported by storm waves at Kudaka Island, Japan. Marine Geology 262, 14–24.
Goto, K., Miyagi, K., Kawamata, H., Imamura, F., 2010. Discrimination of boulders deposited by tsunamis and storm waves at Ishigaki Island, Japan. Marine Geology 269, 34–45.
Heck, N.H., 1947. List of seismic sea waves. Bulletin of the Seismological Society of America 37 (4), 269–286.
Heidarzadeh, M., Pirooz, M.D., Zaker, N.H., Yalciner, A.C., Mokhtari, M., Esmaeily, A., 2008. Historical tsunami in the Makran Subduction Zone off the southern coasts of Iran and Pakistan and results of numerical modeling. Ocean Engineering 35, 774–786.
Heidarzadeh, M., Pirooz, M.D., Zaker, N.H., 2009. Modeling the near-field effects of the worst-case tsunami in the Makran subduction zone. Ocean Engineering 36, 368–376.
Imamura, F., Goto, K., Ohkubo, S., 2008. A numerical model for the transport of a boulder by tsunami. Journal of Geophysical Research 113, CO1008.
Jaiswal, R.K., Singh, A.P., Rastogi, B.K., 2009. Simulation of the Arabian Sea Tsunami propagation generated due to 1945 Makran Earthquake and its effect on western parts of Gujarat (India). Natural Hazards 48, 245–258.
Kelletat, D., Schellmann, G., 2002. Tsunami in Cyprus, field evidence and 14C dating results. Zeitschrift für Geomorphologie 46 (1), 19–34.
Knapp, K.R., Kruk, M.C., Levinson, D.H., Diamond, H.J., Neumann, C.J., 2010. The International Best Track Archive for Climate Stewardship (IBTrACS): unifying tropical cyclone best track data. Bulletin of the American Meteorological Society 91, 363–376.
Kopp, C., Fruehn, J., Flueh, E.R., Reichert, C., Kukowski, N., Bialas, J., Klaeschen, D., 2000. Structure of the Makran subduction zone from wide-angle and reflection seismic data. Tectonophysics 329, 171–191.
Lorang, M.S., 2010. A wave-competence approach to distinguish between boulder and megaclast deposits due to storm waves versus tsunamis. Marine Geology. doi:10.1016/j.margeo.2010.10.005.
Maouche, S., Morhange, C., Meghraoui, M., 2009. Large boulder accumulation on the Algerian coast evidence tsunami events in the western Mediterranean. Marine Geology 262, 96–104.
Mastronuzzi, G., Sansò, P., 2000. Boulders transport by catastrophic waves along the Ionian coast of Apulia (Southern Italy). Marine Geology 170, 93–103.

Mastronuzzi, G., Sansò, P., 2004. Large boulder accumulations by extreme waves along the Adriatic coast of southern Apulia (Italy). Quaternary International 120, 173–184.
Mastronuzzi, G., Pignatelli, C., Sansò, P., Selleri, G., 2007. Boulder accumulations produced by the 20th February 1743 tsunami along the coast of southeastern Salento (Apulia region, Italy). Marine Geology 242, 191–205.
Mokhtari, M., 2005. Seismological aspect and EWS of tsunami prone area of Iranian coasts with special emphases on Makran (Sea of Oman). International Symposium of Disaster Reduction on Coasts Scientific-Sustainable-Holistic-Accessible 14–16 November 2005 Monash University, Melbourne, Australia.
Morhange, C., Marriner, N., Pirazzoli, A., 2006. Evidence of late-Holocene tsunami events in Libanon. Zeitschrift für Geomorphologie 146, 81–95.
Morton, R.A., Richmond, B.M., Jaffe, B.E., Gelfenbaum, G., 2006. Reconnaissance investigation of Caribbean extreme wave deposits; preliminary observations, interpretations, and research directions. Open-File Report 2006–1293, U.S. Department of the Interior. U.S. Geological Survey.
Murty, T., Bapat, A., 1999. Tsunamis on the coastlines of India. Science of Tsunami Hazards 17 (3), 167–172.
Naderi, A., Hamzeh, M., 2010. IOC-UNSCO Field Workshop on Assessment and Awareness of Makran Tsunami Hazards, 9–20 October 2010. Iranian National Institute for Oceanography (INIO), internal report (in Persian). 59 pp.
Nandasena, N.A.K., Paris, R., Tanaka, N., 2011. Reassessment of hydrodynamic equations: minimum flow velocity to initiate boulder transport by high energy events (storms, tsunamis). Marine Geology 281, 70–84.
Noormets, R., Felton, E.A., Crook, K.A.W., 2002. Sedimentology of rocky shorelines: 2. Shoreline megaclasts on the north shore of Oahu, Hawaii: origins and history. Sedimentary Geology 150, 31–45.
Noormets, R., Crook, K.A.W., Felton, E.A., 2004. Sedimentology of rocky shorelines: 3. Hydrodynamics of megaclast emplacement and transport on a shore platform, Oahu, Hawaii. Sedimentary Geology 172, 41–65.
Nott, J.F., 1997. Extremely high-energy wave deposits inside the Great Barrier Reef, Australia: determining the cause; tsunami or tropical cyclone. Marine Geology 141, 193–207.
Nott, J., 2003. Waves, coastal boulder deposits and the importance of the pre-transport setting. Earth and Planetary Science Letters 210, 269–276.
Okal, E.A., Synolakis, C.E., 2008. Far-field tsunami hazard from mega-thrust earthquakes in the Indian Ocean. Geophysical Journal International 172 (3), 995–1015.
Page, W.D., Alt, J.N., Cluff, L.S., Plafker, G., 1979. Evidence for the recurrence of large-magnitude earthquakes along the Makran Coast of Iran and Pakistan. Tectonophysics 52, 533–547.
Pararas-Carayannis, G., 2006a. The potential for tsunami generation along the Makran Subduction Zone in the Northern Arabian Sea. Case study: the earthquake and tsunami of November 28, 1945. Science of Tsunami Hazard 24 (5), 358–384.
Pararas-Carayannis, G., 2006b. Alexander the Great—impact of the 325 BC tsunami in the North Arabian Sea upon his fleet. http://www.drgeorgepc.com/Tsunami325BCIndiaAlexander.html2006.
Paris, R., Fournier, J., Poizot, E., Etienne, S., Morin, J., Lavigne, F., Wassmer, F., 2010. Boulder and fine sediment transport and deposition by the 2004 tsunami in Lhok Nga (western Banda Aceh, Sumatra, Indonesia): a coupled offshore–onshore model. Marine Geology 268, 43–54.
Pignatelli, C., Sansò, P., Mastronuzzi, G., 2009. Evaluation of tsunami flooding using geomorphologic evidence. Marine Geology 260, 6–18.
Prins, M.A., Postma, G., Weltje, G.J., 2000. Controls on terrigenous sediment supply to the Arabian Sea during the late Quaternary: the Makran continental slope. Marine Geology 169, 351–371.
Quittmeyer, R.C., Jacob, K.H., 1979. Historical and modern seismicity of Pakistan, Afghanistan, northwestern India, and southeastern Iran. Bulletin of the Seismological Society of America 69, 773–823.
Rastogi, B.K., Jaiswal, R.K., 2006. A catalog of tsunamis in the Indian Ocean. Science of Tsunami Hazard 25, 128–143.
Regard, V., Bellier, O., Thomas, J.C., Bourlès, D., Bonnet, S., Abbassi, M.R., Braucher, R., Mercier, J., Shabanian, E., Soleymani, Sh., Feghhi, Kh., 2005. Cumulative right-lateral fault slip rate across the Zagros–Makran transfer zone: role of the Minab–Zendan fault system in accommodating Arabia–Eurasia convergence in southeast Iran. Geophysical Journal International 162, 177–203.
Reyss, J.L., Pirazzoli, P.A., Haghipour, A., 1998. Quaternary marine terraces and tectonic uplift rates on the south coast of Iran. In: Stewart, I.S., Vita-Finzi, C. (Eds.), Coastal Tectonics: Geological Society, London, Special Publications, 146, pp. 225–237.
Scheffers, A., 2002. Paleotsunamis in the Caribbean. Field evidences and datings from Aruba, Curaçao and Bonaire. Essener Geographische Arbeiten 33, 183–186.
Scheffers, A., Kelletat, D., 2003. Sedimentologic and geomorphologic tsunami imprints worldwide — a review. Earth-Science Reviews 63, 83–92.
Scheffers, A., Scheffers, S., 2007. Tsunami deposits on the coastline of west Crete (Greece). Earth and Planetary Science Letters 259, 613–624.
Scheffers, A., Kelletat, D., Vött, A., May, S.M., Scheffers, S., 2008. Late Holocene tsunami traces on the western and southern coastlines of the Peloponnesus (Greece). Earth and Planetary Science Letters 269, 271–279.
Scicchitano, G., Monaco, C., Tortorici, L., 2007. Large boulder deposits by tsunami waves along the Ionian coast of south-eastern Sicily (Italy). Marine Geology 238, 75–91.
Southon, J., Kashgarian, M., Fontugne, M., Metivier, B., Yim, W.S., 2002. Marine reservoir corrections for the Indian Ocean and Southeast Asia. Radiocarbon 44, 167–180.
Stuiver, M., Reimer, P.J., Reimer, R., 2005. Calib Radiocarbon calibration, Execute Version 5.0.2. html.http://calib.qub.ac.uk/calib2005.
Suanez, S., Fichaut, B., Magne, R., 2009. Cliff-top storm deposits on Banneg Island, Brittany, France: effects of giant waves in the Eastern Atlantic Ocean. Sedimentary Geology 220, 12–28.
Sunamura, T., Horikawa, K., 1974. Two-dimensional beach transformation due to waves. In: ASCE (Ed.), Proceedings of 14th Coastal Engineering Conference, pp. 920–938.
Switzer, A.D., Burston, J.M., 2010. Competing mechanisms for boulder deposition on the southeast Australian coast. Geomorphology 114, 42–54.
Williams, D.M., Hall, A.M., 2004. Cliff-top megaclast deposits or Ireland, a record of extreme waves in the North Atlantic, storms or tsunamis. Marine Geology 206, 101–117.